Heat Transfer of Microencapsulated PCM Slurry Flow in a Circular Tube

Xichun Wang and Jianlei Niu
Dept. of Building Services Engineering, The Hong Kong Polytechnic University, Hong Kong, P.R. China

Yi Li
Institute of Textiles and Clothing, The Hong Kong Polytechnic University, P.R. China

Yinping Zhang, Xin Wang, Binjiao Chen, and Ruolang Zeng
Dept. of Building Science, Tsinghua University, Beijing 100084, P.R. China

Qingwen Song
Institute of Textiles and Clothing, The Hong Kong Polytechnic University, P.R. China

DOI 10.1002/aic.11431
Published online February 19, 2008 in Wiley InterScience (www.interscience.wiley.com).

Heat transfer characteristics of microencapsulated phase change material (MPCM) slurry flow in a circular horizontal tube are presented in this paper. Phase change due to the melting is investigated for water-based slurries using microencapsulated 1-bromohexadecane ($C_{16}H_{33}Br$) with a mass concentrations varying from 0 to 27.6%. The local heat transfer coefficients varied significantly along the test section when PCM particles were melting. The average Nusselt numbers were calculated based on the local heat transfer data and found to be significantly higher than those for single-phase fluid flow. Two new heat transfer correlations, one used for the slurry under laminar condition ($0 < Re < 2000$) and another used for the slurry under slightly turbulent condition ($2200 < Re < 3500$), were proposed for predicting the heat transfer behaviors of MPCM slurry in a circular tube. © 2008 American Institute of Chemical Engineers *AIChE J,* 54: 1110–1120, 2008

Keywords: MPCM slurry, test section, local Nusselt number, average Nusselt number, phase change

Introduction

The presence of particles such as copper, chalk, carbon, chalk and silica, and plastic bead in single-phase fluids can significantly increase the heat transfer coefficients. Since 1950s, many investigations have been made to understand the heat transfer characteristics of liquid–solid slurries.[1–4] Recent advances in material science have led to the development of new category of fluids termed phase change slurries.[5] Such fluids are liquid suspensions containing a small number of phase change material (PCM) particles with the dimensions of several microns. Because of the high apparent heat capacity induced by the latent heat effect when PCM is melting, phase change slurries may have double benefits of heat transfer augmentation and energy storage relative to conventional solid–liquid slurry flow without phase change, which make it possible to reduce the size of the pipes, heat exchangers, pumps, and thermal storage systems.

Correspondence concerning this article should be addressed to Jianlei Niu at bejlniu@polyu.edu.hk.

Phase change slurries are classified into phase change emulsion and microencapsulated phase change material (MPCM) slurry. The former is prepared by dispersing the fine PCM particles into a single phase carrier fluid, with the additive of emulsifier/surfactant.[6] The latter is produced by microencapsulated fine PCM particles with a thin plastics shell and dispersed into an aqueous solution as a carrier fluid.[7] Because of the sticky properties of the PCM material, particles without microencapsulation easily stick together to form lumps, and clogging may often occur in the pipe systems.[8] However, by microencapsulating the PCM particles, the core material is always separated from the carrier fluid, and therefore the deposition and agglomeration of particles in the slurry are avoided.[9] In addition, the viscosity of MPCM slurry does not increase obviously even when the loading of slurry was increased up to 15%, and the slurry exhibited Newtonian behavior when mass particle fraction is up to 0.3.[10] The MPCM slurry was therefore chosen in this study.

Several studies on the flow and heat transfer characteristics of MPCM slurry flow have been conducted in the past. Kasza and Chen[11] conducted an analytical study to investigate the heat transfer performance of solar energy or waste heat utilization system using phase change slurries and explored the potential benefits in reducing the pumping power and the storage tank size. They claimed that heat transfer performance of slurry flow in both laminar and turbulent conditions would increase because of the microconvective enhancement of thermal conductivity and latent-heat-induced heat capacity. Charunyaorn et al.[12] developed a model to predict the laminar MPCM slurry flow in a heated circular duct and showed about 2–4 times increase of the Nusselt number compared with single phase fluid flow. Goel et al.[13] conducted the heat transfer test of laminar MPCM flow in a heated circular pipe and confirmed the validity of numerical results of Charunyaorn et al. Other related numerical investigations of laminar MPCM slurries flow include the works of Zhang and Faghri,[14] Alisetti and Roy,[15] Hu and Zhang,[16] and Ho et al.[17] All previous investigations in laminar MPCM slurry flow showed that the particle concentration and latent heat were dominating parameters in heat transfer enhancement, whereas the effects of specific heat ratio ($C_{p,p}/C_{p,f}$), thermal conductivity ratio (k_p/k_f), and particle size were relatively weak.

Several experiments were conducted to deal with flow and melting heat transfer characteristics of phase change slurries under turbulent flow conditions in a heated circular duct. Choi et al.[18] measured the local pressure drop and heat transfer coefficient of turbulent phase change emulsion flow (mixture of water and PCM with additive of emulsion) with 10% particle mass concentration in a horizontal tube with constant heating rates. They observed a significant enhancement in heat transfer performance because of the latent heat effect when PCM melted. They also found that both the local heat transfer coefficients and pressure drop along flow direction varied significantly when PCM melted, which made it difficult to apply the log-mean-temperature-difference (LMTD) method to determine the heat transfer coefficient. Yamagishi et al.[19] measured the pressure drop and local convective heat transfer coefficients of turbulent microencapsulated octadecane ($C_{18}H_{38}$) slurry flow in a horizontal circular pipe with constant heating rates, and reported that heat transfer performance of MPCM slurry was influenced by the particle fractions, the degree of turbulence, and the heating rates on the tube wall.

In general, all preliminary studies indicate promising performance of MPCM slurry as a heat transfer and storage medium. No correlations, however, were proposed to describe the melting heat transfer characteristics of MPCM slurry flows in a circular pipe. This is perhaps due to the complex heat transfer mechanisms of the MPCM slurry flow and narrow ranges of experimental conditions applied for each investigation.

This study aims to obtain reliable heat transfer data and derive heat transfer correlations for MPCM slurry flow in a horizontal circular pipe with constant heating rates. The experiments covered both the laminar and turbulent flow velocities and the particle mass fractions varied from 0 to 27.6%. To accurately evaluate the heat transfer characteristics of MPCM slurries in pipes, the average heat transfer coefficients were determined based on the local heat transfer coefficients instead of those based on the inlet and outlet parameters. Numerous correlations of solid–liquid flow without phase change in a horizontal pipe have been reported. In this study, the correlations in the literature will be examined and modified for the specific case of MPCM slurry flow, after which new correlations were developed for the MPCM slurry flow in a horizontal circular pipes with constant heat rates.

Properties of MPCM Slurries

The original MPCM slurry was prepared via a microencapsulation process and consisted of microencapsulated 1-bromohexadecane ($C_{16}H_{33}Br$) particles suspended in pure water. The appearance is shown in Figure 1. The MCPM particles used industrial-grade 1-bromohexadecane (T_m = 14.3°C, ΔH_m = 160 kJ kg^{-1}) as core material and amino plastics as shell material, respectively. The core-shell mass ratio was controlled to about 7:1 during the microencapsulation process. The size distribution of microcapsules was measured by

Figure 1. The appearance of the MPCM slurry developed by the authors.

[Color figure can be viewed in the online issue, which is available at www.interscience.wiley.com.]

a particle characterization system (Malvern Instrument, Malvern Masterzer 2000). As shown in Figure 2, the microencapsulated PCM particle diameter distribution ranged from 2.0 to 31.7 μm and volumetric averaged diameter was 10.1 μm. By diluting the original MPCM with pure water, the less concentrated MPCM slurries could be easily obtained.

The rheological behaviors of the slurry were measured by a Paar Physica MCR 300 Rheometer (Paar Scientific). Figure 3 shows the relationship of share stress and shear rate for the slurries with particle mass fractions from 0.05 to 0.276 at the temperature of 20°C, and it can be seen that the shear stress increased linearly with the rise of the shear rate, and that the lines for different particle mass concentrations crossed at the original point, which proved that the MPCM slurry flow in this study is Newtonian flow even when the particle mass fraction reached 0.276. The measured dynamic viscosities of the slurry at different mass fractions are presented in Table 1.

The densities and heat capacities of slurry were calculated by weighted fraction of the densities of PCM, the coating material, and the water, based on the mass and energy balance.[12]

$$\rho_p = \frac{8}{7}\left(\frac{d_c}{d_p}\right) \tag{1}$$

$$\rho_b = \frac{1}{w_p/\rho_p + (1-w_p)/\rho_w} \tag{2}$$

$$C_{p,b} = w_p C_{p,p} + (1-w_p) C_{p,w} \tag{3}$$

where d_c and d_p are the diameters of the MPCM particle core and MPCM particle, repetitively. w_p is the mass fraction of MPCM particles in the slurry, ρ_p the density of MPCM particles, ρ_w the density of the water, $C_{p,b}$ the specific heat capacity of the slurry, $C_{p,p}$ the specific heat capacity of the MPCM particles, and $C_{p,w}$ the specific heat capacity of the water.

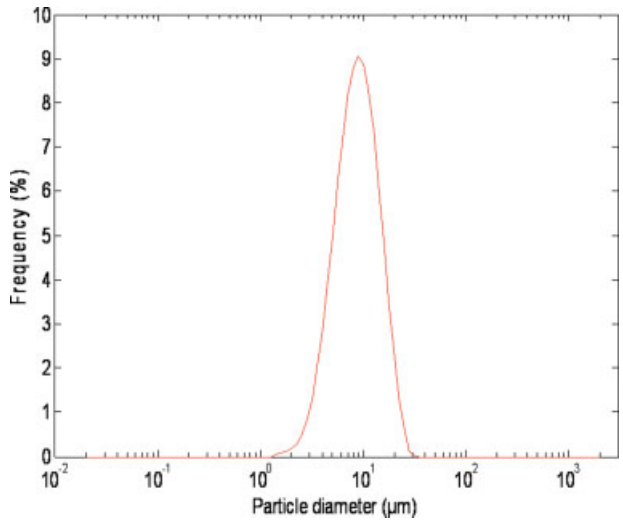

Figure 2. The PCM particle size distribution.

[Color figure can be viewed in the online issue, which is available at www.interscience.wiley.com.]

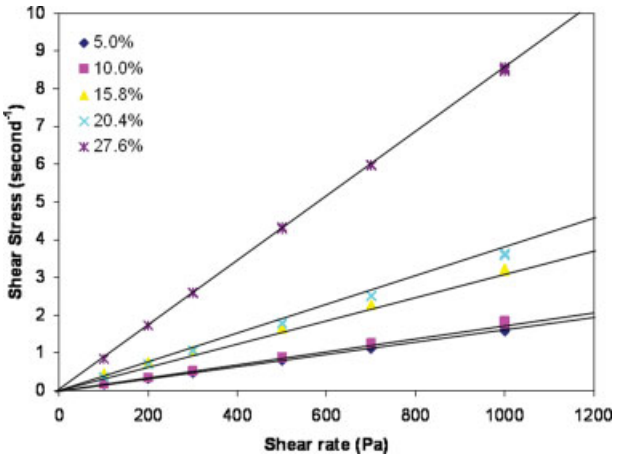

Figure 3. The relationship of shear stress and shear rate at different particle mass concentrations.

[Color figure can be viewed in the online issue, which is available at www.interscience.wiley.com.]

The thermal conductivity of the microcapsule was calculated based on the composite sphere approach,[12] which is given by

$$\frac{1}{k_p d_p} = \frac{1}{k_c d_c} + \frac{d_p - d_c}{k_w d_p d_c} \tag{4}$$

where k_p is the thermal conductivity of the MPCM particles and k_w the thermal conductivity of the water.

The thermal conductivities of MPCM slurries were calculated by Maxwell's relation,[20] which is given as

$$k_b = k_f \times \frac{2k_f + k_p + 2\phi(k_p - k_f)}{2k_f + k_p - \phi(k_p - k_f)} \tag{5}$$

where k_b is the thermal conductivity of the slurry.

The properties of the slurry calculated from Eqs. 1 to 5 are presented in Table 1.

Experimental Details

Experimental apparatus and procedures

An experimental rig was built to study the convective heat transfer feature of the MPCM slurry flows in a horizontal tube. The schematic diagram is shown in Figure 4. The major components include a heat transfer test section, a plate heat exchanger (Tranter, Type B25), a slurry reservoir tank, two slurry pumps, two float flow meters, a AC power supply, and a chiller. The mass flow rate of the slurry was determined by measuring the effluent fluid of the test section by the weighing method.

A 5-l reservoir tank made of polymethylmethacrylate was used to store the MPCM slurry and to monitor the dispersion behavior and the stability of the slurry. To keep the MPCM slurry homogeneous, a variable speed stirrer was installed on top of the tank. The flow rates of slurry were adjusted by tuning a mainline throttling valve and a bypass valve man-

Table 1. Physical Properties of MPCM Slurry and its Components

	Density (kg m^{-3})	Specific Heat (J kg^{-1} $°C^{-1}$)	Thermal Conductivity (W m^{-1} $°C^{-1}$)	Latent Heat (kJ kg^{-1})	Viscosity at 20°C (mPa s)
1-Bromohexadecae					
Solid[21,22]	1006	1762	0.141	160	
Liquid	998	1437	0.300		
Urea-formaldehyde[23]	1490	1675	0.433		
Water (at 20°C)[24]	998	4183	0.599		
MPCM particle					
Solid	1093	1751	0.135	140	1.00
Liquid	1057	1467	0.285		
MPCM slurry (mass fraction)					
$\Phi = 0.050$	1001	4061	0.568	7.0	1.57
$\Phi = 0.100$	1004	3940	0.539	14.0	1.73
$\Phi = 0.158$	1007	3801	0.506	22.0	2.92
$\Phi = 0.204$	1010	3687	0.480	28.6	3.29
$\Phi = 0.276$	1014	3534	0.446	38.6	8.42

ually. A chiller of 3 kW cooling capacity was used to cool the glycol solution. A plate heat exchanger, which has a heat exchanger surface of 1.76 m^2 and heat exchanger capacity of 3 kW, which matches with the capacity of the chiller of 3 kW, was used to freeze the MPCM slurry by the low temperature glycol flow.

The heat transfer test section itself was a straight circular stainless steel (Cri8Ni9Ti) tube, 1.46 m in length with an internal diameter of 4 mm and a wall thickness of 1 mm. It also functioned as the heating source by connecting the electric wire directly on both ends to obtain a uniform heat flux. Power supply consisted of a 3 kVA power transformer, a manually controlled autotransformer and an insulating transformer. The power input to the test section was calculated by multiplying the reading of the ammeter with the reading of the voltage meter. The test section was fitted with flanges, which were isolated electrically and thermally from its upstream and downstream sections by Teflon O-rings. To minimize the heat losses to the ambient environment, the whole test section was thermally insulated by foam-type insulation material with a thickness of 10 cm.

The inlet and outlet slurry temperatures of the test section were measured by inserting the PT-1000 type thermocouples into the flowing fluid. The thermocouples for measuring the inlet and outlet were located 10 cm upstream and downstream of the heat transfer test section. The measuring points of the two thermocouples were located at the center points between the inner tube wall surface and the tube centerline. The measuring point for the slurry outlet bulk temperature was fully hydraulically developed because the length of the entrance region starting from the inlet of the test tube can be calculated by the equations of $L_{\text{laminar}} = 0.05\ Re_b\ D_{\text{tube}}$ and $L_{\text{turbulent}} = 10 D_{\text{tube}}$, respectively, for the laminar and turbulent flows. On the other hand, there is no axial heat conduction because the inlet and outlet heated sections of test tube were insulated by the Teflon flange. Therefore, there were minimal radial temperature gradients in the slurry flow at the cross section of the measure point. Theoretically, this careful location of the thermocouple for measuring the outlet bulk temperature as already rendered has the reading very close to the outlet bulk temperature of the slurry.

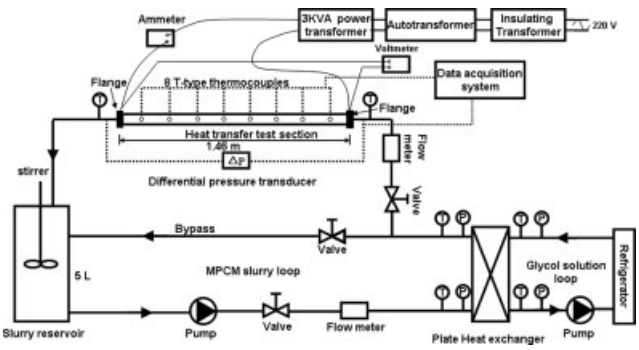

Figure 4. Schematic diagram of the experimental apparatus.

Eight T-type thermal couples were attached to the outer surface of the test tube and the distance between the neighboring points was 0.18 m. The inlet and outlet temperatures of heat exchangers were measured by inserting four T-type thermal couples into the fluids. All the temperature sensors were calibrated and the measurement error was less than 0.1°C. Pressure drop was measured across the test section using an electronic differential pressure transducer with an accuracy of ±0.01 kPa. During the experiments, the variations of the temperatures at the inlet and outlet of test section were controlled to be less than ±0.25°C. Four pressure gages were also installed in the inlet and outlet of the heat exchangers for each pass to monitor the pressure variations.

To estimate the heat loss from the experimental apparatus to the ambient environment, the apparatus was firstly operated with only pure water flowing in the system. Then the heat losses can be estimated by subtracting the net heat removal by the water flow from the electric power inputs of the AC power supply. The experiments were repeated with different electrical power inputs and fluid mass flow rates. The heat losses to the surroundings were found to be small (maximum 4% to the total electric power input).

When the MPCM slurry flowed in the system, the temperatures at the outlet of the heat exchanger were controlled at 2°C by tuning the inlet temperature of the glycol solution, which was much lower than the melting temperature of the

PCM (T_m = 14.3°C). Considering the supercooling degree of 10°C, such a low temperature was necessary to solidify all the PCM in the heat exchanger. When the slurry temperature and flow rate were set at the desired values, the electric power was switched on to heat the slurry flow. The outlet temperatures of the test section were controlled at 20 or 25°C to ensure that all PCM particles have completed the phase change processes by adjusting the electrical power input to the test section. In normal working conditions, the slurry at the inlet of heat exchanger was pressurized by the pressure pump to about 0.65 MPa to overcome frictions in both the heat exchanger and the main test section.

All data from different instruments were taken after reaching the steady state by observing the temporal variations in the slurry inlet and outlet temperatures, test tube surface temperatures, pressure drop, and power input. Data points were taken at 10 min interval during steady state. All the data were directly stored in the computer through a HP-34970 data acquisition system.

Data analysis method

The heat loss over the test section to the environment was evaluated by the following equation:

$$Q_{loss} = Q_{input} - \dot{m}C_{p,b}(T_{b,o} - T_{b,i}) \quad (6)$$

where Q_{input} is the electric power imposed on the test section, $\dot{m}$ and $C_{p,b}$ are the mass flow rate and specific heat capacity of the water, respectively, and T_{in} and T_{out} are the inlet and outlet of the water temperatures.

In this investigation, the local heat transfer coefficient between the inner wall tube surface and the slurry flow was defined as

$$h_x = \frac{q_{lw}}{T_{lw} - T_{lb}} \quad (7)$$

where q_{lw} is the local heat flux at the tube wall, T_{lw} is the local inner wall surface temperature, and T_{lb} is the local bulk mean temperature of the fluid. The local bulk mean temperature of the water can be easily calculated by assuming linear increase along the test section, based on the inlet and outlet temperatures and the tube heat flux. However, the local bulk mean temperature of the fluid accompanying phase change is not linear, and thus it cannot be simply estimated from the aforementioned method. In this experiment, the local bulk mean temperatures were calculated based on the "three-region melting model," which was proposed by Choi et al.,[6] and the model is quite dependent of the material property data. Table 2 shows the derived equations for the determination of the length of each region and associated bulk mean temperature profile, $T_b(x)$.

Based on the energy balance, the latent heat of the slurry flowing in the test tube can be calculated by the following equation:

$$\Delta H_m = \left[\frac{L_1 + L_2}{L}Q - \dot{m}(T_m - T_{b,i})\right] \Big/ \dot{m} \quad (8)$$

To ascertain the complete phase change process and check the accuracy of the measured outlet bulk temperature of slurry, the calculated latent heat value by Eq. 8 at each experimental run was compared with that measured using the DSC technique, because the latent heat value is always constant for specific kind of MPCM slurry.

Table 2. Bulk Temperature Profile Equation and Length of Each Region

	Local Bulk-Mean Temperature	Length of the Regions
Region I	$T_b(x) = T_{bi} + \frac{Q}{\dot{m}C_{p,b}}\frac{x}{L}$	$\frac{L_1}{L} = \frac{\dot{m}C_{p,b}(T_m - T_{b,i})}{Q}$
Region II	$T_b(x) = T_m$	$\frac{L_2}{L} = \frac{L - L_1 - L_3}{L}$
Region III	$T_b(x) = T_m + \frac{Q}{\dot{m}C_{p,b}}\frac{x}{L}$	$\frac{L_3}{L} = \frac{\dot{m}C_{p,b}(T_{b,o} - T_{m,})}{Q}$

The inner tube wall surface temperature, T_{lw}, was derived from the model based on 1-D thermal conduction in the homogeneously heated wall of the test section,[25] and the result is given as

$$T_{lw} = T_{wo} - C_1\frac{q_{lw}}{k_{wo}}\left(1 + \frac{C_1}{2}\frac{aq_{lw}}{k_{wo}^2}\right) \quad (9)$$

where

$$C_1 = \frac{r_w}{r_{wo}^2 - r_w^2}\left(r_{wo}^2 \ln\frac{r_{wo}}{r_w} - \frac{r_{wo}^2 - r_w^2}{2}\right)$$

T_{wo} is the tube outer wall surface temperatures. r_w and r_{wo} are the wall inside and outside radii, respectively. k_{wo} is the thermal conductivity of the tube, k_{wo} = 14.235 + 0.013398 T_{wo}, and a = 0.0144, which is a constant.

Thermal conductivity, viscosity, and density of the slurry can be evaluated from the physical property data in Table 1, and the local dimensionless numbers for MPCM slurry flowing in the heat tube were defined as follows:

$$Nu_x = h_x D/k_b \quad Pr_{lb} = C_{p,b}\mu_b/k_b \quad Re_{lb} = Du_m\rho_b/\mu_b \quad (10)$$

Instead of the LMTD method, the average heat transfer coefficient (h_m), Nusselt number (Nu_m), Prandtl number (Pr_m) and Reynolds number (Re_m) were calculated using the arithmetic averages of the local values in this study.

Uncertainty analysis

The maximum error of the temperature reading in this study was 1.0%, and the error in the measurements of the inner/outer diameter and pipe length was 0.5%. The mass flow rate of the slurry was calculated from the mass of the effluent fluid of the test section over a certain period, which had an error of 0.1%. The error in the measurements of voltage and current were 1.5% and 1.0%, respectively. The error in viscosity measurement was 1.0%. The corresponding uncertainty for the Reynolds number therefore was 1.12%.

Because of the radial temperature gradient in the tube, the bulk mean temperatures of the slurry inside the test tube were not directly measured but calculated by the "three-region melting model." There might be deviations between the calculated value and real value. To estimate the extent of this deviation, the bulk temperature of the slurry can also be calculated by "the linear melting model," which assumes a linear melting process of the MPCM particles both in Region I and Region II. The actual melting processes might have the

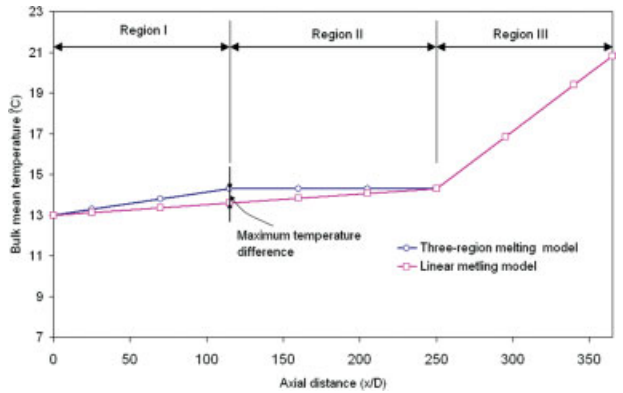

Figure 5. Two models for the bulk-mean temperature of the MPCM slurry.

[Color figure can be viewed in the online issue, which is available at www.interscience.wiley.com.]

bulk temperature values between two extremes calculated by the above two proposed models. This is also confirmed by Yamagishi et al.,[19] who directly measured the local bulk temperatures of the microencapsulated octadecane slurry under turbulent flow conditions by five thermocouples, all local bulk temperatures in the Region I and Region II lied in the two extremes calculated by the two models, and the measured bulk temperatures were much more close to the bulk temperature calculated by "three-region melting model." Figure 5 shows the bulk-mean temperature of slurry calculated by the two models, and the bulk mean temperature calculated by the "three-region melting model" is always higher than that calculated by the "linear melting model." Therefore, the heat transfer coefficient calculated by the three-region model is higher than that by the "linear melting model." This adds uncertainty for determining the heat transfer coefficient. However, in our experiments the inlet temperature of the slurry was controlled to be slightly lower than the melting temperature. As a result, in the axial position where the maximum temperature difference would occur, the mean bulk temperature calculated by the "three-region melting model" is no more than 3.5% higher than that calculated by the "linear melting model" for all the experimental runs, and this will result in an additional 3.5% uncertainty in the heat transfer coefficient calculation.

The errors of the input heat flux measurements mainly depend on the accuracies of the ammeter, the voltmeter, and the heat loss from the section to the environment. The total heat loss of the test section, which was calculated by Eq. 6, was less than 4% of the electric power input from the AC power supply. Therefore, the uncertainty for local heat transfer coefficient was ±6.7%, and the corresponding uncertainty of Nusselt number was ± 6.7%. The deviation between the calculated latent heat of the slurry for each experimental run was less than 4%, which can be considered as the error caused by the heat loss of the test section.

Results and Discussion

Local heat transfer characteristics

In Figure 6, the evolution of the local Nusselt Number, Nu_x, is plotted against the dimensionless axial distance, $x/(r_D RePr)$, at particle mass concentrations of w_p = 5%, 10% and 15.8%, and under the same heating rate across the test section, Q = 296.8 W, and the same mass flow rate, $\dot{m}$ = 4.95 g s^{-1}. The corresponding Nusselt numbers for pure water under the same heating rate and mass flow rate were also calculated by Eq. 10, which is given for the single-phase laminar flow in the thermally developing region[26] as follows:

$$Nu_x = 5.364\left[1+\left(\frac{200x^*}{\pi}\right)^{-10/9}\right]^{3/10} - 1.0$$

where

$$x^* = (x/D)/(Re_{lb}\, Pr_{lb}) \tag{11}$$

D is the tube inner diameter, x is the axial distance from the inlet of test section, Re_{lb} local Reynolds number of the bulk liquid slurry, and Pr_{lb} local Prandtl number of the bulb liquid slurry.

As is shown in Figure 6, when the mass particle concentration w_p = 15.8%, the local Nusselt number increased up to 60.4% in comparison with single-phase flow. Such enhancement was also related to the particle mass concentration, and the Nusselt number increased with the particle mass concentrations. The local Nusselt number varied significantly along the flow direction. The local heat transfer coefficient decreased until all PCM particles melted, after that it increased slightly, and finally it almost remained constant. It is also interesting to note that the local Nusselt number difference between the MPCM slurry flow and the pure water flow increased along the flow direction before the dimensionless axial location of 0.02, and after that the difference decreased till the point of 0.037, then it increased slightly and it almost remained constant finally. Such phenomena can be explained by the latent heat effect on the heat transfer behaviors. The PCM particles firstly melted near the pipe wall at the entrance of heat transfer section, as more particle melting, the heat transfer coefficient increased, when the number of melting particles reached at a maximum value at the dimensionless axial point of 0.02, the heat transfer coefficient reached maximum value. After that the number of melt-

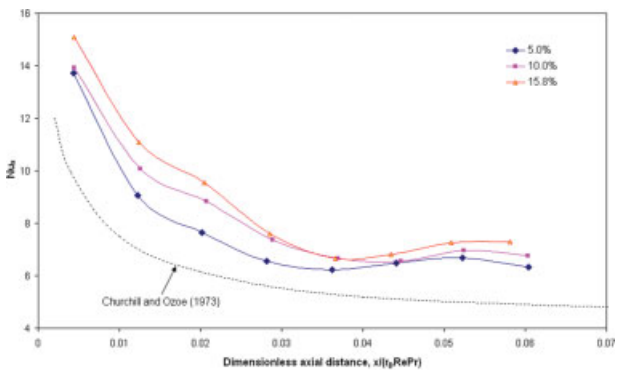

Figure 6. The effects of particle mass fraction on local Nusselt number.

[Color figure can be viewed in the online issue, which is available at www.interscience.wiley.com.]

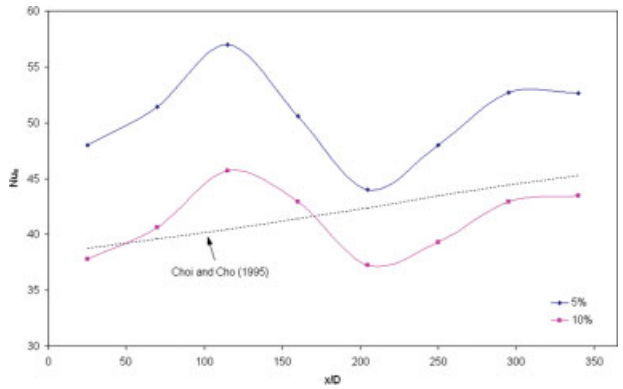

Figure 7. Local Nusselt numbers at different particle mass concentrations of 5% and 10% Re_{lb} = 4285–6201 for water and Re_{lb} = 2515–3738 for slurry at $\dot{m}$ = 18.2 g s^{-1}.

[Color figure can be viewed in the online issue, which is available at www.interscience.wiley.com.]

ing PCM particle decreased gradually, and so did the heat transfer coefficient. When all PCM particles melted at the point of 0.037, the heat transfer coefficient of MPCM slurry approached that for the pure water. After the completion of the melting, the viscosity decreased and Reynolds number increased due to the increased temperature of slurry along the test section, which result in a slight increase of the local Nusselt number.

Figure 7 compares the heat transfer performance of MPCM slurry at two different particle mass concentrations, while the mean mass flow rate, the inlet temperature, and heating rate are the same for two cases. The dashed line in Figure 7 shows the local Nusselt number calculated by using Eq. 12, which was derived by Choi and Cho[27] for the turbulent convective heat transfer of a single-phase fluid with combined thermal developing and hydraulic developed regions at the constant heating rates.

$$Nu_x = 0.00425\, Re_{lb}^{0.979} Pr_{lb}^{0.4} (\mu_{lw}/\mu_{lb})^{-0.11} \qquad (12)$$

where water dynamic viscosity μ_{lb} was evaluated based on the local mean temperature of the fluid and water dynamic viscosity, μ_{lw}, was calculated based on the local wall inner surface temperature.

As is shown in Figure 7, the local Nusselt number varied significantly along the heat transfer section. The Nusselt number increased before the axial location of x/d = 115, then decreased till the point of x/d = 205, and increased again after that, while the local Nusselt number for pure water increased almost linearly along the heat transfer section. Such phenomena can be explained as follows: the PCM particles melted near the tube wall at the entrance of the test section, and as more PCM particles are melting, the heat transfer coefficient increased. As the number of melting particles reached the maximum value at the point of x/d = 115, the corresponding heat transfer coefficient also reached the maximum value. After that the number of melting particles decreased gradually, and on the other hand, the melted PCM particles near the tube wall prevented the transport of solid PCM particles to the tube wall surface, both of which reduce the possibility of melting PCM particles, and hence the heat transfer coefficient also decreased. When all the PCM have completed the melting at the point of x/d = 205, the Nusselt number increased slightly again after that because of the increased slurry temperature along the test section.

In Figure 7, it is interesting to notice that the local Nusselt numbers of the slurry with w_p = 10% were lower than those of the slurry with w_p = 5%, and even lower than those of pure water in some locations. Yamagishi et al.[19] also found a similar phenomena in a turbulent microencapsulated octadecane ($C_{18}H_{38}$) slurry flow, which contradicted with heat transfer augmentation by the latent heat effect and microconvective thermal conductivity enhancement. While, the heat transfer characteristics of turbulent MPCM slurry flow is influenced not only by the latent heat and enhanced thermal conductivity, but also by the turbulent degree. As reported by Liu et al.,[28] there is a threshold of particle size in the augmentation of the heat transfer of a fluid when it was added into a single-phase flow. When the particles are smaller than such size, a degradation of heat transfer will be achieved. On the other hand, when particles size is bigger than such size, there will be an enhancement in heat transfer performance for a specific test tube. The higher loadings of the solid particle will further degrade the heat transfer performance. The very fine particles used in this study (d_m = 10.1 μm) tended to follow all eddies and promote the laminar flow condition, especially at higher particle concentrations, which results in the reduction of turbulent degree of the slurry flow. When the heat transfer degradation due to the presence of the fine particles exceeds the heat transfer enhancement due to the latent heat effects of the MPCM cores, a lower heat transfer coefficient of slurry compared with that of water appeared. The higher local Nusselt number relative to the pure water in Figure 7 for the case of w_p = 10% particle concentrations exactly reflected the latent heat effect of PCM during phase change, although the lower local Nusselt number relative to pure water were found for almost 2/3 of the pipe length because of the depression of turbulence.

Average heat transfer characteristics

Figure 8 illustrates the tendency of the average Nusselt numbers of laminar MPCM slurry at different mass fractions of PCM particles and the Reynolds numbers. The experimental results indicate that MPCM slurry remarkably improve heat transfer performance of the carrier fluid. Compared with pure water, the Nusselt number of MPCM slurry was increased more than 45% with particle mass fraction of 5% at the same Reynolds number. Heat transfer enhancement up to 167% was achieved when particle mass fraction was 0.276. The experimental results also indicate that the heat transfer augmentation of MPCM slurry significantly increased with the mass faction of PCM particles and the Reynolds numbers. Therefore the particle mass fraction and Reynolds number are dominating parameters affecting the Nusselt numbers of a slurry flow.

The average heat transfer coefficients were also calculated using the correlation given by Stephan,[29] which is given for a simultaneously developing single-phase laminar flow (*Re*

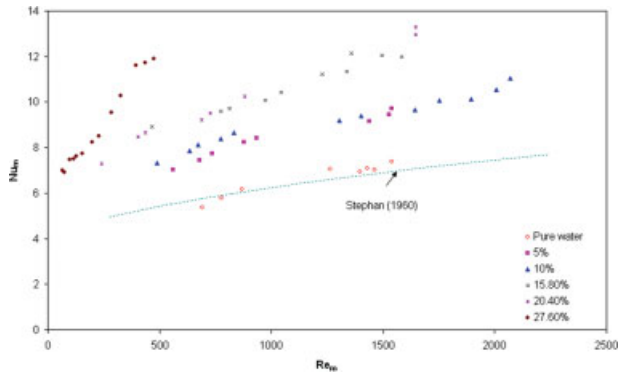

Figure 8. The Nusselt numbers of laminar MPCM slurry vs. the Reynolds numbers and the predicted values from Stephan correlation.

[Color figure can be viewed in the online issue, which is available at www.interscience.wiley.com.]

< 2300) in a circular tube under constant wall heat flux as follows:

$$Nu_f = 4.364 + \frac{0.086\left(RePr\frac{D}{L}\right)^{1.33}}{1 + Pr\left(Re\frac{D}{L}\right)^{0.83}} \tag{13}$$

The comparison between the present experimental results and predicted values from Stephan's correlation for single phase-phase flow is shown in Figure 8. It was observed that the discrepancies between the experimental values and predicted values were less than 6%. Considering the experimental difficulties experienced with the heat transfer of the fluid, these results should be acceptable.

The average MPCM slurry Nusselt numbers in turbulent flow are plotted in Figure 9 for runs conducted at two different particle mass concentrations. The average heat transfer coefficients are also predicted by the correlation given by Gnielinski,[30] which can accurately predict the fully developed single-phase flow for the Reynolds Number from 2300 to 10^4 in a circular pipe under uniform heat flux conditions as follows:

$$Nu_{gn,m} = \frac{(f/8)\left(Re_D - 1000\right)Pr}{1 + 12.7(f/8)^{1/2}\left(Pr^{2/3} - 1\right)} \tag{14}$$

where

$$f = \left(1.82\ \log_{10} Re_D - 1.64\right)^{-2}$$

As shown in Figure 9, the discrepancies between predicted values and the present experimental values were less than 8%, and the experimental values for pure water were always higher than the predicted values. This is perhaps due to the improper use of the Gnielinski correlation to calculate the heat transfer coefficient. Gnielinski correlation is suitable for fully developed turbulent flow, while the water flow here was confined in thermally developing and hydraulically developed flow region.

Figure 9 suggests that enhanced heat transfer performance was achieved for slurries with particle concentrations of both 5 and 10%; about 1–2.5 times higher average Nusselt number relative to those of water was obtained in comparison with single-phase flow. Unsurprisingly, the lower average heat transfer coefficients for 10% slurry relative to 5% slurry were also found in Figure 9 because of the suppression of turbulence of the MPCM slurry flow. In some cases, the average heat transfer coefficients for 10% slurry approached to water at the same flow conditions.

Heat transfer correlations

The dimensionless correlations are required for the design purposes to predict the convective heat transfer of MPCM slurry in a horizontal circular tube. Because of the presence of microencapsulated PCM particles in the water, correlation equations for a single-phase flow, however, failed to predict the heat transfer behaviors of MPCM slurry, and hence new correlations should be proposed.

Several empirical correlations have been reported to predict the heat transfer characteristics of solid–liquid flow without phase change in the pipes. Salamone and Newman[1] investigated the heat transfer of the water suspensions of solid particles of copper, carbon, chalk, and silica with various size ranges from 1.5 to 56 μm and with concentrations varying from 2.3% to 10.7% (by volume) in a horizontal pipe and derived the following correlation:

$$Nu = 0.131\ Re^{0.62}Pr^{0.72}\left(\frac{k_p}{k_f}\right)^{0.05}\left(\frac{D}{d_p}\right)^{0.05}\left(\frac{C_{p,p}}{C_{p,f}}\right)^{0.35} \tag{15}$$

for $14{,}000 \le Re \le 140{,}000$, $3.4 \le Pr \le 12.7$, $0.53 \le k_p/k_f \le 12.7$, $282 \le D/d_p \le 10{,}500$, and $0.09 \le C_{p,p}/C_{p,f} \le 0.22$.

Harada et al.[3] also investigated the water suspensions of glass beads with particle diameters varying from 0.06 to 1.0 mm in volume fraction of 0–10% in a horizontal pipe. However, their experimental data could not be fitted well by the Salamone and Newman correlation because of the different kinds of particles used in each investigation. Based on the Sieder-Tate equation, the following correlation was proposed.

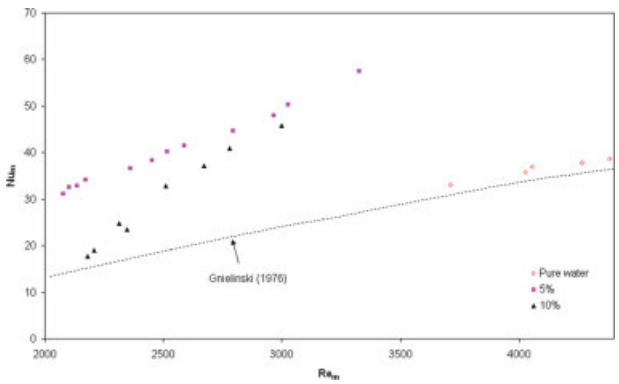

Figure 9. The Nusselt number of turbulent MPCM slurry vs. the Reynolds number and predicted values from Gnielinski correlation.

[Color figure can be viewed in the online issue, which is available at www.interscience.wiley.com.]

$$Nu = 1.6 \times 10^{-2} Re^{0.88} Pr^{1/3} \left(\frac{\mu_f}{\mu_w}\right)^{0.14} \quad (16)$$

for $8000 \leq Re \leq 50{,}000$, $0.01 \leq \dot{m} \leq 0.1$, and $0.0024 \leq d/D \leq 0.071$. The accuracy of the correlation is approximately $\pm 15\%$.

On the basis of experimental data, Özbelge and Somer[31] derived a correlation for heat transfer to dilute liquid–solid flow in a horizontal pipe, which is given as

$$Nu = 0.202 Re^{0.6} Pr^{0.675} \left(\frac{D}{d_p}\right)^{0.092} \left(\frac{\mu_f}{\mu_w}\right)^{-1.95} \quad (17)$$

for $27{,}000 \leq Re \leq 120{,}000$, $2.1 \leq Pr \leq 3.4$, $1.17 \leq \mu_f/\mu_w \leq 1.83$, $\leq D/d_p \leq 512$, and $0.5\% \leq w_p \leq 3\%$. The accuracy of the correlation is $\sim 20\%$.

In this work, because of the presence of the MPCM particles in the fluid, the heat transfer process can be divided into two distinguished regions, the regions with phase change and without phase change. The corresponding heat transfer coefficient of two regions can be obtained separately. The average heat transfer coefficients of slurry without phase change can be calculated by Eqs. 15–17. The average heat transfer equations for solid–liquid slurry with phase change will be obtained based on the present experimental data.

Although Eqs. 15–17 were not consistent because of different experimental conditions and particular slurry used, they can be expressed with a function of $Nu = f(Re, Pr, D/d_p, k_p/k_f, C_{p,p}/C_{p,f}, \mu_s/\mu_w)$ in general. According to our literature review of the investigation of MPCM slurries, particle diameter, thermal conductivity ratio, and heat capacity ratio have little effect on the heat transfer characteristics, because of the presence of the microencapsulated PCM particles in the slurry; however, the latent heat of the material and the heat flux imposed on the test tube significantly influence the phase change process of the MPCM particles along the flow direction slurry in the test tube, and thus affect the heat transfer performance of the slurry. The latent heat and heat flux effects can be described by a dimensionless parameter Stefan number,[12] which is defined as

$$Ste = \frac{C_{p,b}|q_w R_d/k_b|}{w_p \Delta H_m \rho_p/\rho_b} \quad (18)$$

where R_d is the radius of the test tube.

The phase change region $(L_1 + L_2)$ of the MPCM particles can be described as a dimensionless parameter $(L_1 + L_2)/D$. Therefore a general form of $Nu = f[Re, Pr, Ste, (L_1 + L_2)/D, \mu_s/\mu_w]$ is obtained in this investigation to describe the heat transfer characteristics of MPCM slurry in the phase change region of the test tube.

For laminar MPCM slurry flow, the following dimensionless parameters are used to account the effect of microencapsulated PCM particles in the laminar flow: average Reynolds (Re_m), Prandtl number (Pr_m), Stefan number (Ste), and phase change region length $[(L_1+L_2)/D]$. A linear model was proposed based on the regression analysis of heat transfer coefficient data. The coefficients of the proposed model were determined by the least square method,[32] which yields the following correlation equation giving best fit with the present experimental data for $60 < Re_m < 2200$, $12 < Pr_m < 73$ and $0.05 < w_p < 0.276$.

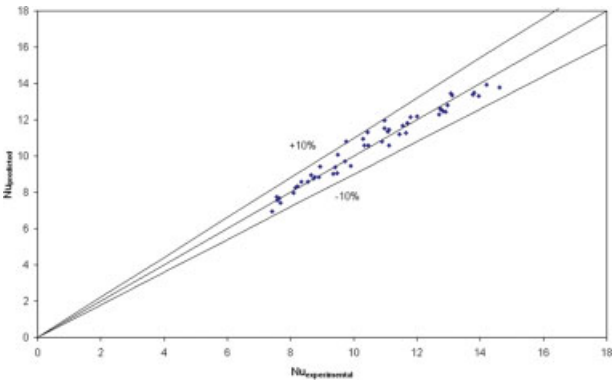

Figure 10. Comparison of measured and predicted Nusselt numbers for laminar MPCM slurry flow.

[Color figure can be viewed in the online issue, which is available at www.interscience.wiley.com.]

$$Nu_m = 0.8148 Re_m^{0.4593} Pr_m^{0.4836} Ste^{-0.1277} [(L_1+L_2)/D]^{0.3059} \quad (19)$$

As can been seen from Eq. 19, the heat transfer correlation equation of slurry in the phase change region has negative powers of Stefan number and phase change region length and positive powers of Reynolds number and Prandtl number. This quite accords with the phenomena presented in Figure 8, and the average heat transfer coefficient increases with the amount of PCM particles suspended in the water.

Figure 10 compares the experimental heat transfer results with those predicted by Eq. 19, and all the experimental data can be predicted by Eq. 19 with a standard deviation within $\pm 10\%$.

For the turbulent MPCM slurry flow, dimensionless analysis was also used in the derivation of heat transfer correlation. The first four groups are the average Reynolds number (Re_m), average Prandtl number (Pr_m), and the phase change region length $[(L_1 + L_2)/D)]$. The dimensionless group (μ_s/μ_w) is a correction factor to account for the effect of wall temperature on the heat transfer coefficient. The coefficients of proposed regression model were determined by the least square method, which yielded the following correlation giving the best fit with the present experimental data for $2100 < Re < 3500$, $13 < Pr < 15$, and $0.05 < w_p < 0.1$.

$$Nu_m = 4.8527 \times 10^{-4} {Re_m}^{0.7733} {Pr_m}^{2.7941} Ste^{0.3159} \times [(L_1 + L_2)/D]^{-0.333} (\mu_m/\mu_w)^{-2.4349} \quad (20)$$

where μ_m is the average dynamic viscosity of the slurry in the phase change region and μ_w the average dynamic viscosity of water calculated based on the inner tube wall temperature.

Figure 11 compares the experimental heat transfer results with those predicted by Eq. 20, and all the data can be predicted with Eq. 20 with a standard deviation within ± 10 %.

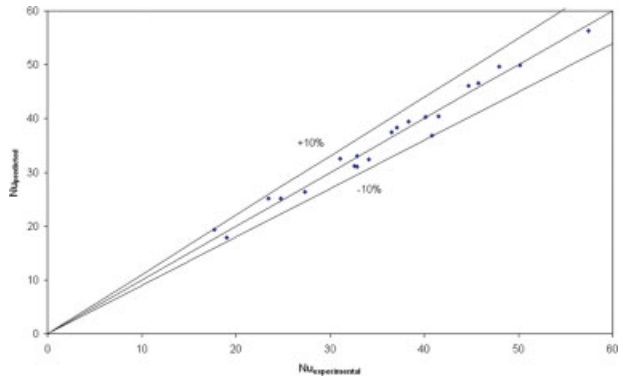

Figure 11. Comparison of measured and predicted Nusselt numbers for turbulent MPCM slurry flow.

[Color figure can be viewed in the online issue, which is available at www.interscience.wiley.com.]

Equation 20 differs from the Eqs. 15–17, which can be explained by as follows.

Equations 15–17 were obtained at very high Reynolds number without phase change, while the present experiments covered slightly turbulent flow ($2100 < Re < 3500$) and latent effect of the MPCM particles. Although the higher power of 0.7733 of Reynolds number in Eq. 20 is similar to the power of 0.62–0.88 in Eqs. 15–17, the power of Prandtl number is much higher than those presented in the previous equations due to the low thermal conductivity of the MPCM particles. On the other hand, because of the latent heat effect of slurry with suspended MPCM particles, the latent heat item and length of phase change region are included in Eq. 20.

In this work, the particle mass fraction takes negative effect on the heat transfer coefficient, and the fine MPCM particle decreases the turbulent degree of slurry under turbulent flow conditions; this phenomena can also be found in Figure 8. This effect is also reflected by a pronounced negative power of the viscosity ratio in Eq. 20. According to our present manufacturing technique of MPCM particles, particle size of 1–30 μm only can be produced. With the development of the microencapsulation technique, the effect of particle size on the heat transfer performance of slurry along the horizontal test tube will be examined in our future research.

Conclusions

An experimental study was performed to investigate the heat transfer characteristics of MPCM slurries in a circular horizontal tube with constant heating rates. The local heat transfer coefficients were measured at both laminar and turbulent flow conditions. It is found that the local heat transfer behaviors varied significant along the flow direction of the slurry. The average heat transfer coefficients were also calculated based on the local heat transfer data. Results showed that local heat transfer coefficients for laminar slurry flow were always higher than those of single-phase fluid because of the latent heat effect and microconvective thermal conductivity enhancement, whereas the heat transfer performance of turbulent slurry flow are not only affected by the above two factors, but are greatly influenced by turbulent degree. About 1–2.5 times higher average Nusselt number relative to pure water was found for turbulent slurry flow, whereas a degradation of heat transfer performance was found at a higher particle load of the slurry.

The heat transfer behaviors were modeled by applying appropriate properties modified from the correlations for solid–liquid mixture without phase-change effect. A new laminar heat transfer correlation using dimensionless groups was proposed for slurry in the phase change region along the test tube direction, which predicts the average heat transfer data within an error of $\pm 10\%$. A new turbulent heat transfer correlation using dimensionless group was also proposed, which predicts the average heat transfer data with standard deviation within $\pm 10\%$. The new correlations, derived based on the series of experiments covering in both laminar and turbulent flow conditions, should be useful for the design of the new compact heat exchangers with MPCM slurry applications.

Acknowledgments

The authors are grateful to the Innovation Technology Commission and the Hong Kong Polytechnic University for providing support to this research through ITS-023-03, ITS-049-06, and A188. This work was also partially supported by the Research Grant Council of the Hong Kong SAR government (Project No. 5255/06).

Notation

a = constant (Eq. 8) (W m $^{\circ}C^2$)
C_p = specific heat capacity (J kg^{-1} K^{-1})
d = particle diameter (μm)
D = tube diameter (m)
Gz = Graetz number
H = heat transfer coefficient (W m^{-2} $^{\circ}$C^{-1})
ΔH = latent heat of fusion (kJ kg^{-1})
k = thermal conductivity (W m^{-1} K^{-1})
L = length of test section, length of the entry section (m)
$\dot{m}$ = mass flow rate (g s^{-1})
Nu = Nusselt number
Pr = Prandtl number
ΔP = pressure drop (kPa)
q = heat flux (W m^{-2})
Q = heat rate (W)
r = radius of the test tube (m)
Re = Reynolds Number
T = temperature ($^{\circ}$C)
ΔT = temperature difference ($^{\circ}$C)
u = flow velocity (m s^{-1})
w = mass faction
x = coordinate in the axial direction (m)

Greek letters

P = density (kg m^{-3})
Φ = volumetric fraction
η = dynamic viscosity (mPa s)

Subscripts

c = microcapsule core
b = bulk
f = fluid
i = inlet
lb = based on local bulk temperature
lw = based on local wall temperature
m = mean, melting point

o = outlet
p = particle
w = wall
wo = external wall surface
x = location in the axial direction
1–3 = melting regions of slurry in tube

Literature Cited

1. Salamone JJ, Newman M. Heat transfer design characteristics: water suspensions of solids. *Ind Eng Chem*. 1955;47:283–288.
2. Ahuja AS. Augmentation of heat transport in laminar flow of polystyrene suspensions. I. Experiment and results. *J Appl Phys*. 1975; 46:3408–3416.
3. Harada E, Toda M, Kuriyama M, Konno H. Heat transfer between wall and solid-water suspension flow in horizontal pipes. *J Chem Eng Jpn*. 1975;18:33–38.
4. Sohn CW, Chen MM. Microconvective thermal conductivity in disperse two-phase mixture as observed in a low velocity Couette flow experiment. *J Heat Transfer*. 1981;103:47–50.
5. Kasza KE, Chen MM. *Development of enhanced heat transfer/transport/storage slurries for thermal system improvement*. ANL-82-50, Argonne National Laboratory, IL, 1982.
6. Choi E, Cho YI, Lorsch HG. Effects of emulsifier on particle size of a phase change material in a mixture water. *Int Commun Heat Mass Transfer*. 1991;18:759–766.
7. Roy SK, Sengupta S. An evaluation of phase change microcapsules for use in enhanced heat transfer fluids. *Int Commun Heat Mass Transfer*. 1991;18:459–450.
8. Winters PJ. Phase two laboratory testing of direct freeze ice slurry district cooing. Final report, DOE contract no. DE-FG01-88CE26559, 1991.
9. Inaba H. New challenge in advanced thermal energy transportation using functionally thermal fluids. *Int J Thermal Sci*. 2000;39:991–1003.
10. Yang R, Xu H, Zhang Y. Preparation, physical property and thermal physical property of phase change microcapsule slurry and phase change emulsion. *Solar Energy Mater Solar Cells*. 2003;80:405–416.
11. Kasza KE, Chen MM. Improvement of the performance of solar energy or waste heat utilization systems by using phase-change slurry as an enhancement heat-transfer storage fluid. *J Solar Energy Eng*. 1985;107:229–236.
12. Charunyaorn P, Sengupta S, Roy SK. Forced convective heat transfer in microencapsulated phase change material slurries: flow in circular ducts. *Int J Heat Mass Transfer*. 1991;34:819–833.
13. Goel M, Roy SK, Sengupta S. Laminar forced convection heat transfer in microencapsulated phase change material suspensions. *Int J Heat Mass Transfer*. 1994;37:593–604.
14. Zhang Y, Faghri A. Analysis of forced convection heat transfer in microencapsulated phase change material suspensions. *J Thermophys Heat Transfer*. 1995;9:727–732.
15. Alisetti EL, Roy SK. Forced convection heat transfer to phase change materials slurries in circular ducts. *J Thermophys*. 1999;14: 115–118.
16. Hu X, Zhang Y. Novel insight and numerical analysis of convective heat transfer enhancement with microencapsulated phase change material slurries: laminar flow in a circular tube with constant heat flux. *Int J Heat Mass Transfer*. 2002;45:171–190.
17. Ho CJ, Lin JF, Chiu SY. Heat transfer of solid-liquid phase-change material suspensions in circular pipes: effects of wall conduction. *Numer Heat Transfer A*. 2004;45:171–190.
18. Choi E, Cho YI, Lorsch HG. Forced convection heat transfer with phase-change-material slurries: turbulent flow in a circular tube. *Int J Heat Mass Transfer*. 1993;37:207–215.
19. Yamagishi Y, Takeuchi H, Pyatenko AT. Characteristics of microencapsulated PCM slurry as a heat-transfer fluid. *AIChE J*. 1999; 45:696–707.
20. Maxell JC. *A Treatise on Electricity and Magnetism*, *3rd ed*. New York: Dover Publications, 1954:440–441.
21. Holmen R, Lamvik M, Melhus O. Measurements of thermal conductivities of solid and liquid unbranched alkanes in the C16-to-C19 range during phase transition. *Int J Thermophys*. 2002;23:27–39.
22. Yaws L. *Yaws' Handbook Thermodynamic and Physical Properties of Chemical Compounds*. New York: Knovel, 2003.
23. Dean JA. *Lange's Handbook of Chemistry*, *15th ed*. New York: McGraw-Hill, 1999.
24. Bejan A, Kraus AD. *Heat Transfer Handbook*. New Jersey: Wiley, 2004.
25. Allen RW, Eckert ERG. Friction and heat-transfer measurements to turbulent pipe flow of water (Pr = 7 and 8) at uniform wall heat flux. *J Heat Transfer*. 1964;86:301–310.
26. Churchill SW, Ozoe H. Correlations for forced convection with uniform heating flow over a plate and in developing and fully developed flow in a tube. *J Heat Transfer*. 1973;95:78–84.
27. Choi E, Cho YI. Local friction and heat transfer behavior of water in a turbulent pipe flow with large heat flux at the wall. *J Heat Transfer*. 1995;7:283–288.
28. Liu KV, Choi US, Kasza KE. Pressure drop and heat transfer characteristics of nearly neutrally buoyant particulate slurry for advanced energy transmission fluids. In: Proceedings of the Third International Symposium on Liquid-Solid Flows, 1988:107–113.
29. Stephan K. Wärmeübergang und Druckabfall bei nicht ausgebildeter Laminarströmung in Rohren und ebenen Spalten. *Chem-Ing-Tech*. 1959;31:773–778.
30. Gnielinski V. New equations for heat and mass transfer in turbulent pipe and channel flow. *Int Chem Eng*. 1976;16:359–368.
31. Özbelge TA, Somer TG. A heat transfer correlation for liquid-solid flows in horizontal pipes. *Chem Eng J*. 1994;55:39–44.
32. Watson GS. Serial correlation in regression analysis I. *Biometrika*. 1955;42:327–341.

Manuscript received Apr. 17, 2007, and revision received Dec. 17, 2007.